Electronic Supplementary Material (ESI) for Journal of Materials Chemistry C.
This journal is © The Royal Society of Chemistry 2017

Supporting Information

Inversion of the charge carrier polarity and boosting the mobility of organic semiconducting polymers based on benzobisthiadiazole derivatives by fluorination

Yang Wang*, Aaron Tze-Rue Tan, Takehiko Mori and Tsuyoshi Michinobu*

Department of Materials Science and Engineering, Tokyo Institute of Technology, 2-12-1 Ookayama, Meguro-ku, Tokyo 152-8552, Japan

*Corresponding address:
Yang Wang
Tel/Fax: +81-3-5734-2469, E-mail: wang.y.av@m.titech.ac.jp

Tsuyoshi Michinobu
Tel/Fax: +81-3-5734-3774, E-mail: michinobu.t.aa@m.titech.ac.jp

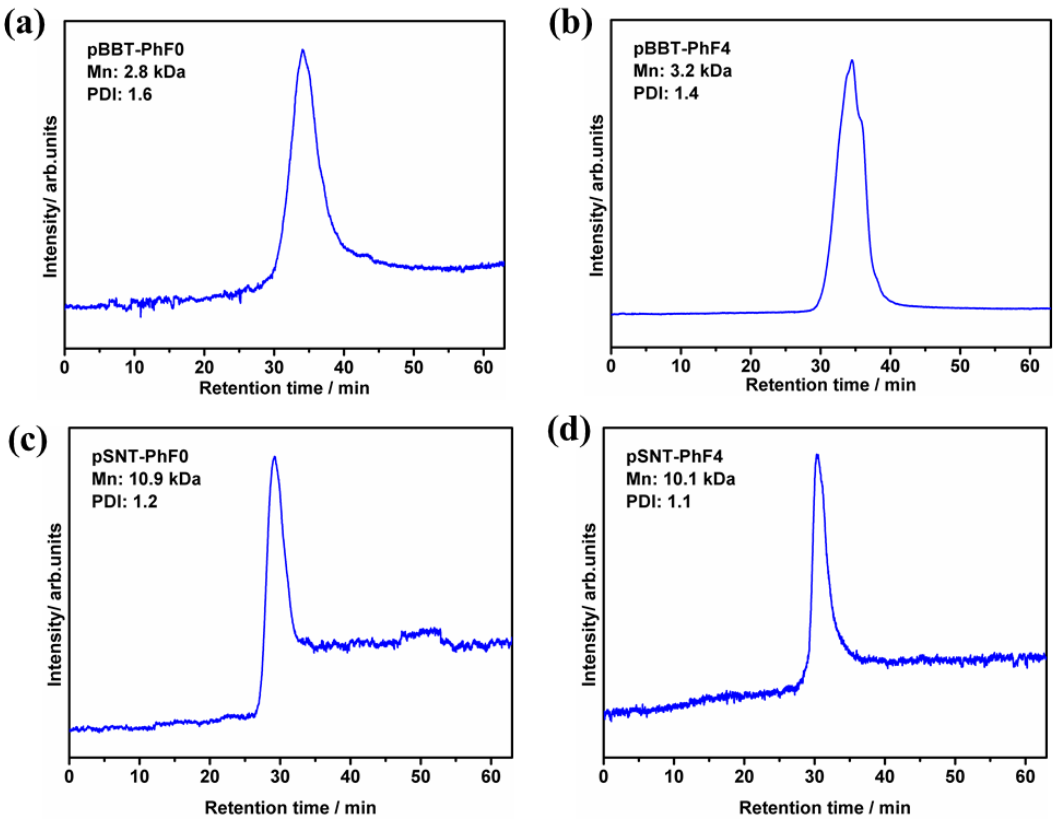

Fig. S1 GPC curves of (a) pBBT-PhF0, (b) pBBT- PhF4, (c) pSNT-PhF0, and (d) pSNT-PhF4 using 1,2-dichlorobenzene as the eluent at 40 °C. Polystyrene standards were used to estimate the molecular weights.

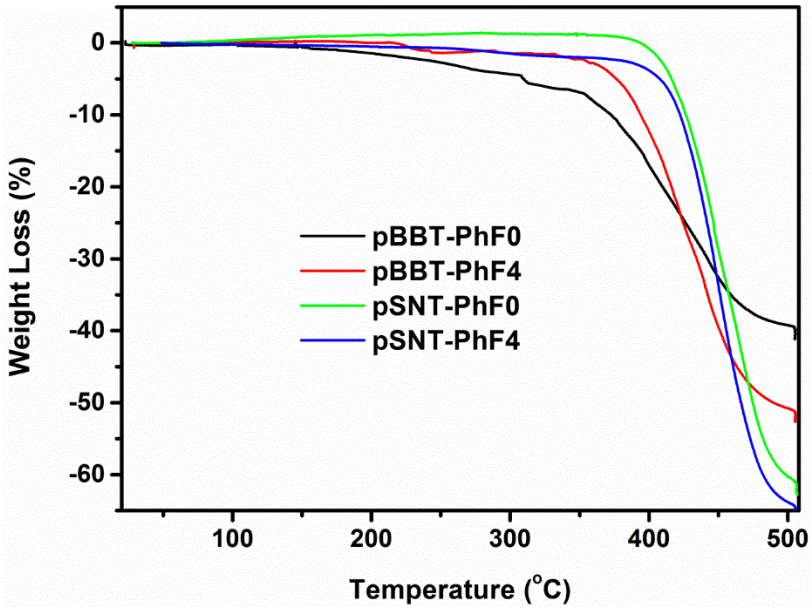

Fig. S2 Thermogravimetric analysis (TGA) curves of the copolymers under nitrogen atmosphere at the heating rate of 10 °C min^{-1}.

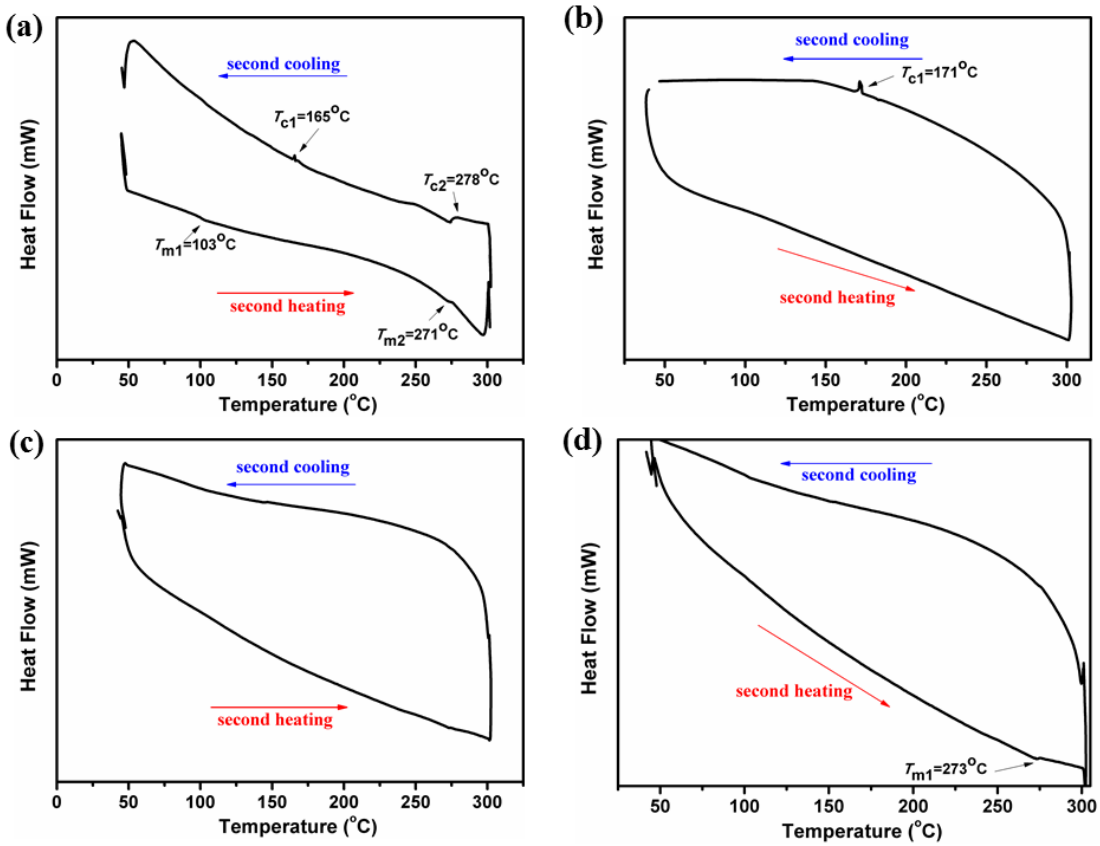

Fig. S3 Differential scanning calorimetry (DSC) curves of (a) pBBT-PhF0, (b) pBBT-PhF4, (c) pSNT-PhF0, and (d) pSNT-PhF4. All the DSC curves are the second heating and cooling processes under nitrogen flow (50 mL min^{-1}) at the scan rate of 10 °C min^{-1}.

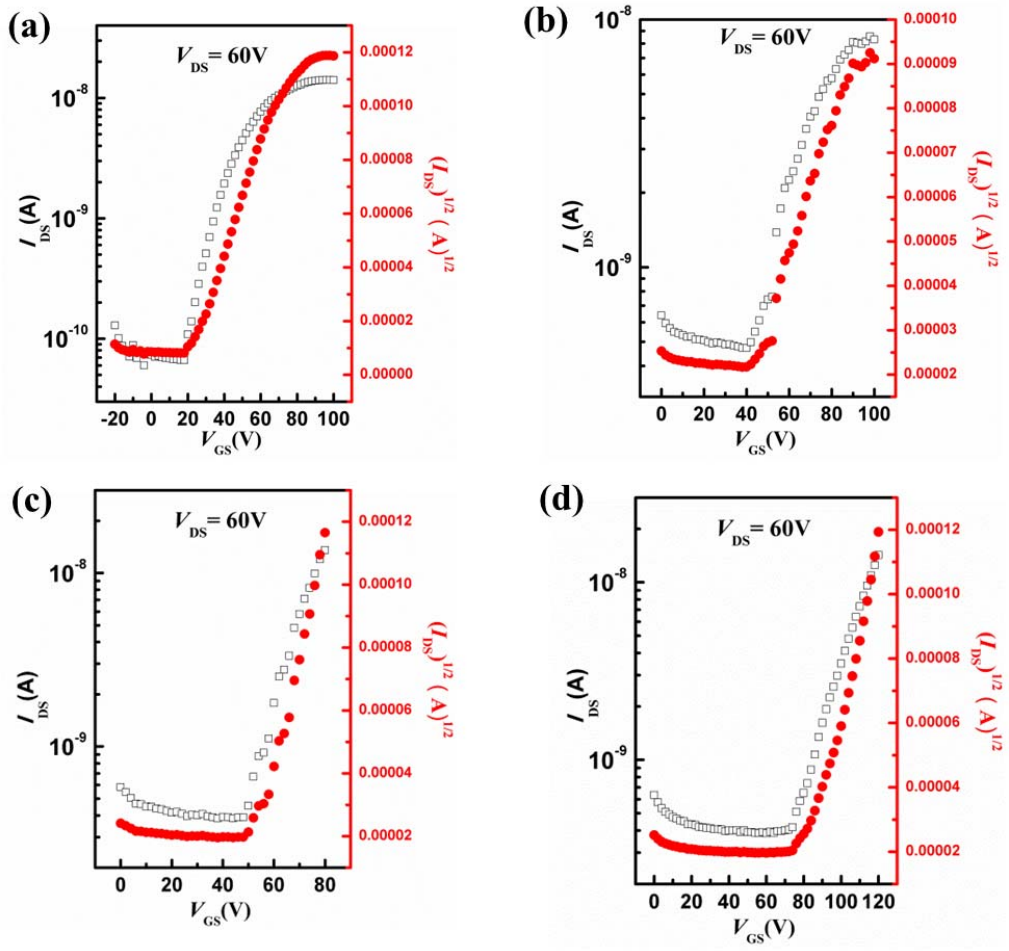

Fig. S4 Thermal annealing temperature dependent current−voltage (*I*−*V*) characteristics of pBBT-PhF4-based TFTs (a) without thermal annealing; (b) with thermal annealing at 100 ^{o}C; (c) with thermal annealing at 125 ^{o}C; and (d) with thermal annealing at 175 ^{o}C (electron-enhancement operation with V_{DS} = 60 V, L = 100 μm and W = 1 mm, measured in a vacuum chamber with a pressure of 10^{-4} mbar).

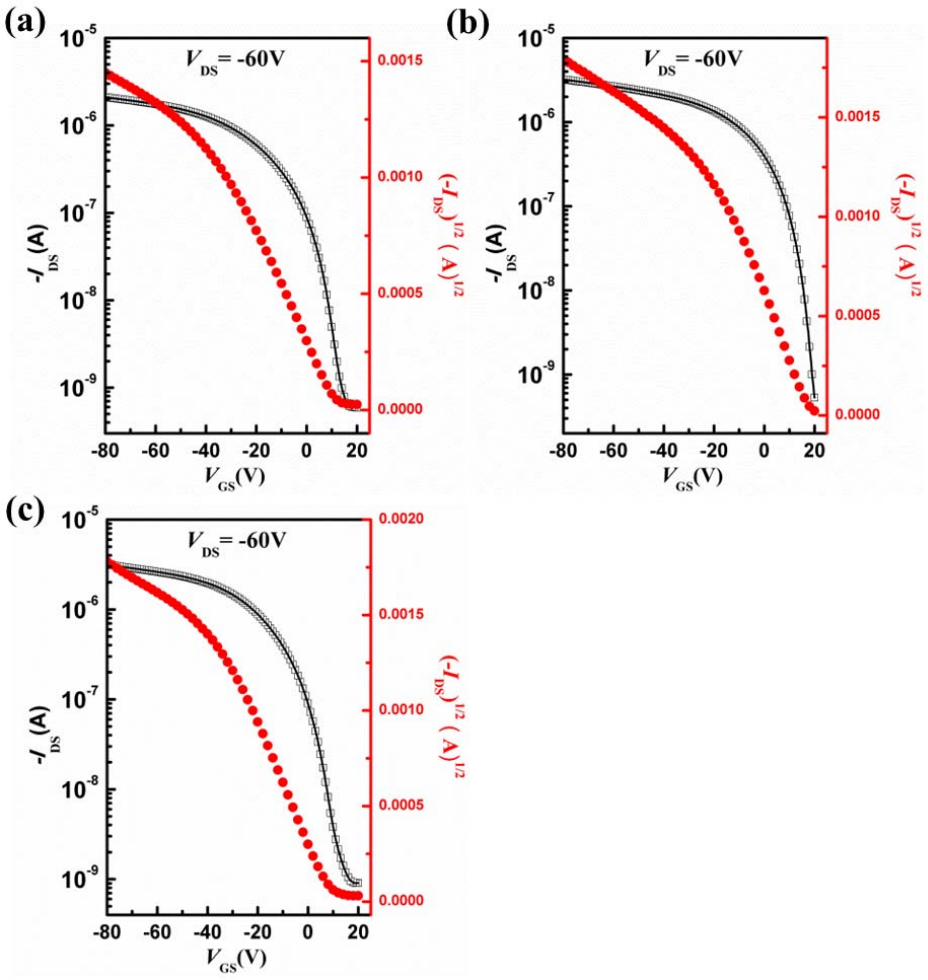

Fig. S5 Thermal annealing temperature dependent current−voltage (*I*−*V*) characteristics of pSNT-PhF0-based TFTs (a) without thermal annealing; (b) with thermal annealing at 150 °C; and (c) with thermal annealing at 250 °C (hole-enhancement operation with V_{DS} = −60 V, L = 100 μm and W = 1 mm, measured in air).

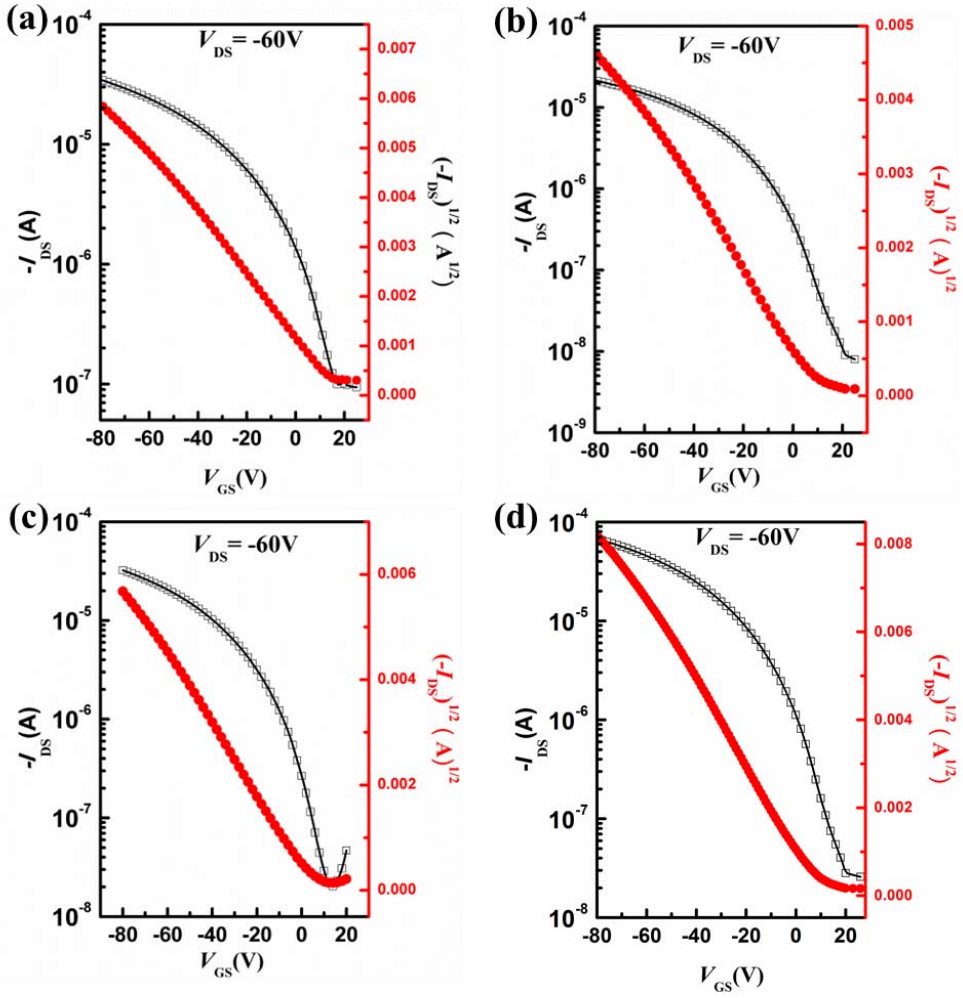

Fig. S6 Thermal annealing temperature dependent current−voltage (*I*−*V*) characteristics of pSNT-PhF4-based TFTs (a) without thermal annealing; (b) with thermal annealing at 150 °C; (c) with thermal annealing at 200 °C; and (d) with thermal annealing at 200 °C (hole-enhancement operation with V_{DS} = −60 V, *L* = 100 μm and *W* = 1 mm, measured in air).

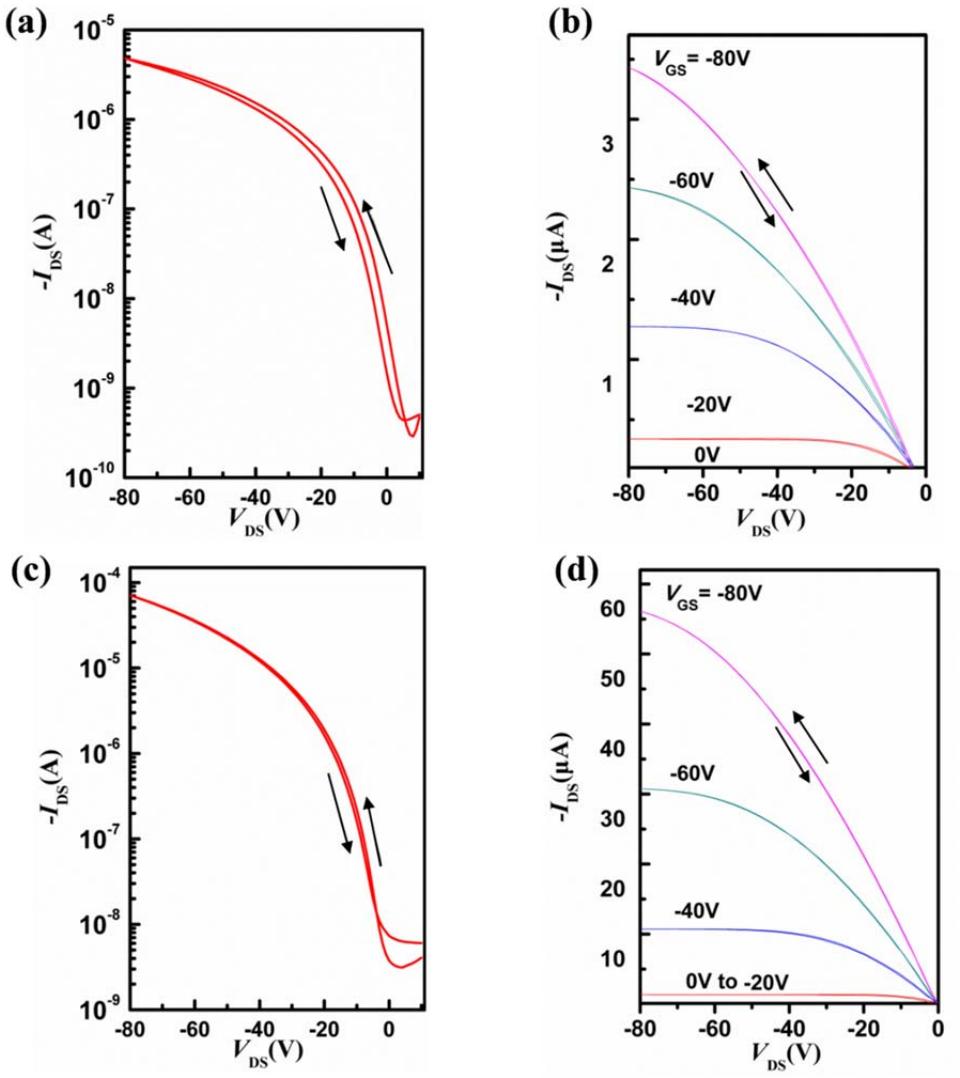

Fig. S7 The hysteresis test of the TFT devices: (a) forward and reverse curves of the transfer characteristics of pSNT-PhF0; (b) forward and reverse curves of the output characteristics of pSNT-PhF0; (c) forward and reverse curves of the transfer characteristics of pSNT-PhF4; (d) forward and reverse curves of the output characteristics of pSNT-PhF4.

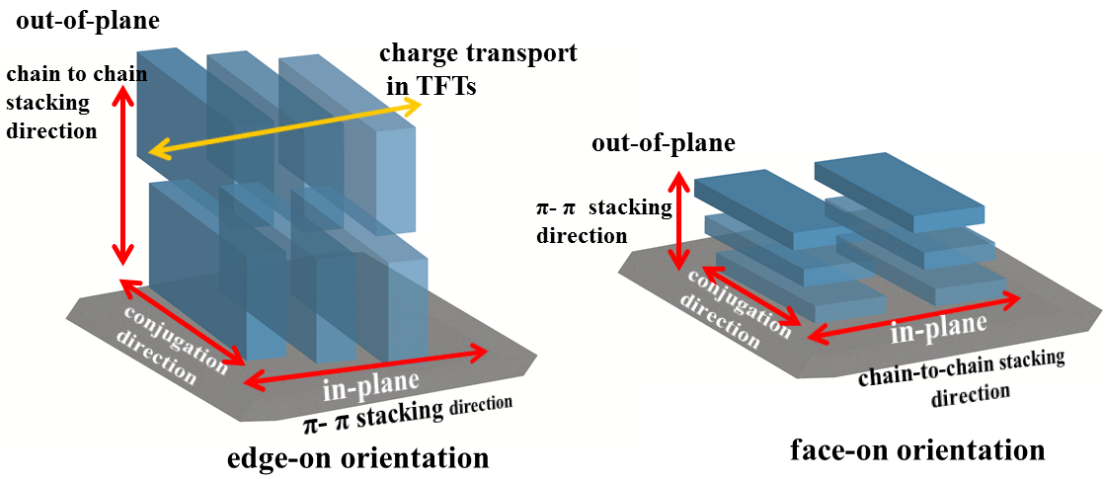

Fig. S8 Schematic illustration of the charge transport model in lamellar stacking conjugated polymers. Left: edge-on texture of polymeric crystallites; Right: face-on texture of polymeric crystallites.

NMR charts

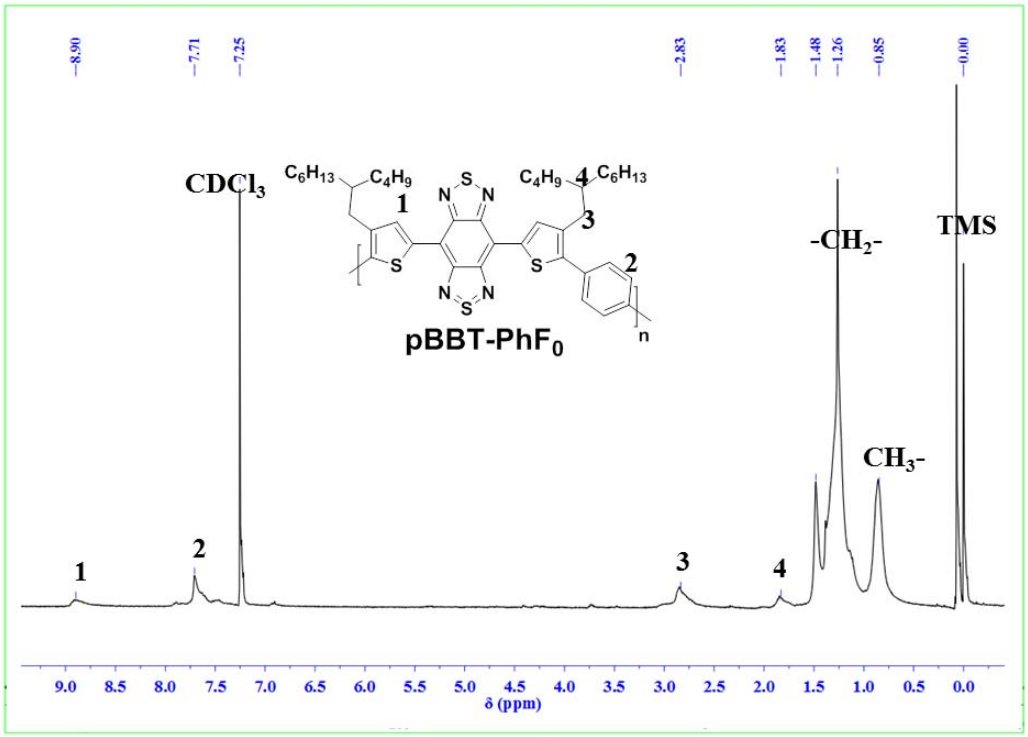

Fig. S9 ^{1}H NMR spectrum of pBBT-PhF0 in $CDCl_3$.

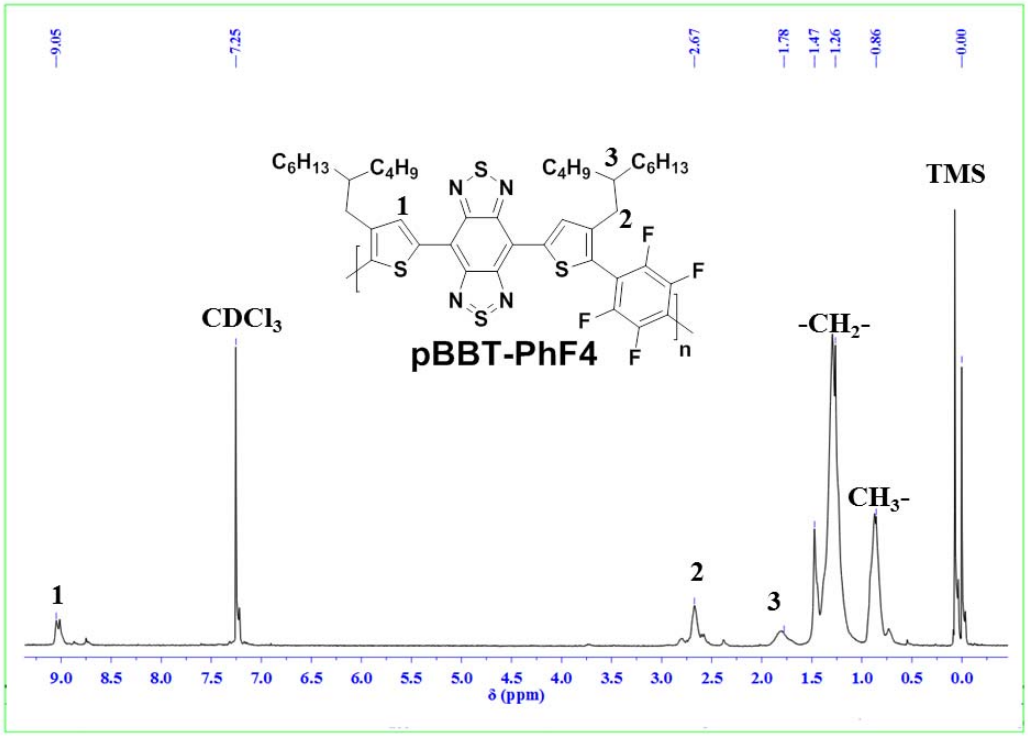

Fig. S10 ^{1}H NMR spectrum of pBBT-PhF4 in $CDCl_3$.

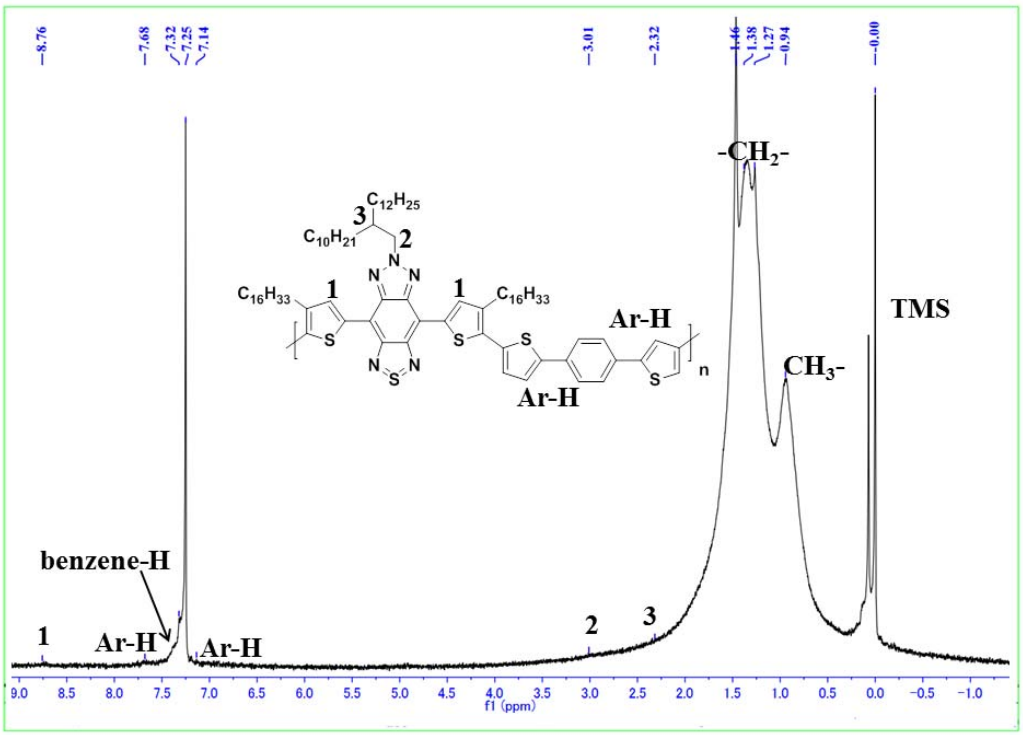

Fig. S11 ^{1}H NMR spectrum of pSNT-PhF0 in $CDCl_3$.

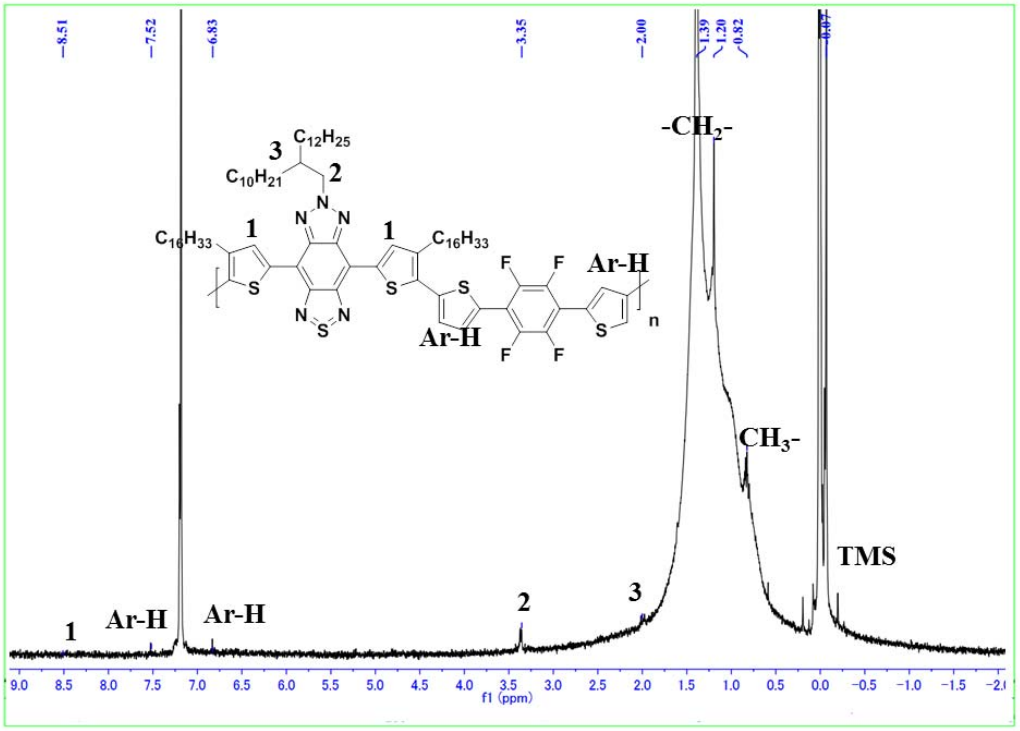

Fig. S12 ^{1}H NMR spectrum of pSNT-PhF4 in $CDCl_3$.